Int. J. Electrochem. Sci., 12 **(2017)** 2606 – 2617, doi: 10.20964/2017.03.54

International Journal of
ELECTROCHEMICAL
SCIENCE
www.electrochemsci.org

High Performance Symmetric Supercapacitor Based on Sunflower Marrow Carbon Electrode Material

KanjunSun[1,2,*], *Qian Yang*[2], *YanpingZheng*[1], *GuohuZhao*[1], *YanrongZhu*[1], *XiaopingZheng*[1], *GuofuMa*[2,*]

[1] College of Chemistry and Environmental Science, Lanzhou City University, Lanzhou 730070, China.
[2] Key Laboratory of Eco-Environment-Related Polymer Materials of Ministry of Education, Key Laboratory of Polymer Materials of Gansu Province, College of Chemistry and Chemical Engineering, Northwest Normal University, Lanzhou 730070, China.
[*]E-mail: sunkj@lzcn.edu.cn, magf@nwnu.edu.cn
Qian Yang and Kanjun Sun contributed equally to this work.

Received: 28 October 2016 / *Accepted:* 19 January 2017 / *Published:* 12 February 2017

In this study, sunflower marrow is used as raw material to prepare porous carbon via a simple carbonization method activated by $ZnCl_2$ and $FeCl_3$ mixture. The as-prepared porous sunflower marrow carbons (PSMCs) show large number of mesoporous and masoporous, maximum specific surface area of 1628.5 m^2 g^{-1} and large pore volume of 2.34 cm^3 g^{-1}. As an electrode material for supercapacitor, the PSMCs possess high specific capacitance of 252.5 F g^{-1} at 0.5 A g^{-1}. A symmetric supercapacitor used PSMCs as electrodes exhibits energies density of 12.4 Wh kg^{-1} at a power density of 817 W kg^{-1} operated in the voltage range of 0-2.0 V in 0.5 mol L^{-1} Na_2SO_4 aqueous electrolyte. Also, the carbon material shows excellent cycleability retains about 97% initial capacitance after 5000 cycles.

Keywords: Sunflower marrow, Porous carbon, Supercapacitors

1. INTRODUCTION

It is a necessary solution to response the increasing energy shortage and concomitant environmental pressure to explore reliable, sustainable and efficient energy source forms free of pollution emission [1-3]. Supercapacitors, also known as electrochemical capacitor, have attracted more and more attention due to the advantages of high power density, faster charging-discharging rate, longer cycling life and better operation safety over other secondary batteries. For all of these, supercapacitors are thought to be as an important type of energy storage and supply devices [4-7]. According the mechanisms, supercapacitor can be divided in two types, the electrcal double-layer

capacitor (EDLCs) and pseudo-capacitors. The EDLCs store energy is based on electrostatic attraction at the electrode/electrolyte interface to generate charge accumulation in the electric double layers, while pseudo-capacitors store energy by the fast and reversible redox reactions at the surface of the active electrode materials [8-10]. Currently, the final electrochemical performance of the EDLCs depends on the chemical and physical properties of the electrode material. A lot of carbon materials have been prepared as EDLCs electrodes, especially, template carbons [11,12], carbon nanotubes [13,14] and graphene [15,16], and biomass porous carbons also the material of choice due to their low cost and large availability.

Recently, biomass, as green, renewable and efficient energy source, has become of great interest to use for energy available in large quantities around the world. In particular, biomass material lignocellulosic, an economical and eco-friendly energy source, is composed mainly of hemicelluloses, lignin, and cellulose, and does not compete with the food chain [17]. Redondo et al. used olive pits as starting material to prepare nanoporous carbon with a specific capacitance as high as 260 F g^{-1}. The good electrochemical performance of the carbon was attributed to a well developed porosity and textural properties of carbon materials [18]. Chen et al. (2012) prepared an activated carbon material for electrode of supercapacitor from cotton stalk active by phosphoric acid (H_3PO_4). The carbon developed has a high specific surface area, the capacitance values is 114 F g^{-1}, due to the surface chemistry characteristics and pore structures of activated carbons [19]. Wang et al. prepared biomass-based activated carbons as electrode materials for supercapacitors from willow catkins by KOH chemical activation. The carbon displays excellent electrochemical properties, for example, the specific capacitance is as high as 340 F g^{-1} and high specific surface capacitance is 52.7 mF cm^{-2} at the current density of 0.1 A g^{-1}, due to the large specific surface area, moderate pore size distribution and rich nitrogen and oxygen containing functional groups on the suface [20].

As is known, the sunflower is one of the most important agricultural commodities in the world. There are 2,500,000 tons of wastes per year in the form of sunflower stalks, which is a serious problem for farmers growing sunflower [21]. In this paper, sunflower marrow which is the inner of sunflower stalks composed primarily of lignocellulosic was used as raw material to prepare activated carbon electrode. Different activation strategies have been applied to prepare different carbons for supercapacitors. The porous sunflower marrow carbons (PSMCs) were prepared by $ZnCl_2$ and $FeCl_3$ to improve the pore structures, surface chemistry performances. In addition, the relationship between the surface chemistry characteristics, pore structures, and the capacitance of PSMCs have been discussed in detail.

2. EXPERIMENTAL

2.1 Materials

Sunflower marrow (SM, Lanzhou city of Gan Su province, China); Zinc Chloride ($ZnCl_2$, Aladdin Ltd., China); Ferric Chloride ($FeCl_3$, Shanghai Chemical Works, China). All other chemical reagents were in analytical grade.

2.2 Synthesis of porous activated carbon networks (PSMCs)

The porous sunflower marrow carbons (PSMCs) were prepared via carbonization route activated by $ZnCl_2$ and $FeCl_3$. Firstly, 1.0 g sunflower marrow, 2.0 g $ZnCl_2$ and 20 mL 0-3 M $FeCl_3$ solution were mixed under stirring to form a homogeneous solution. Then the solution was then transferred into a flask and kept in a oil bath at 100 ^oC under vigorous stirring to completely evaporate solvent. Secondly, the dried solid samples were carbonized at 800 ^oC for 2 h in a tube furnace under a nitrogen atmosphere, then the products were washed in 10 wt% HCl and deionized water to remove metal ions till the filtrate became neutral. Finally, the resulting PSMCs was obtained afer dried at 60 ^oC in an oven 24 h. The facile entire procedure for preparing PSMCs as described in Scheme 1.

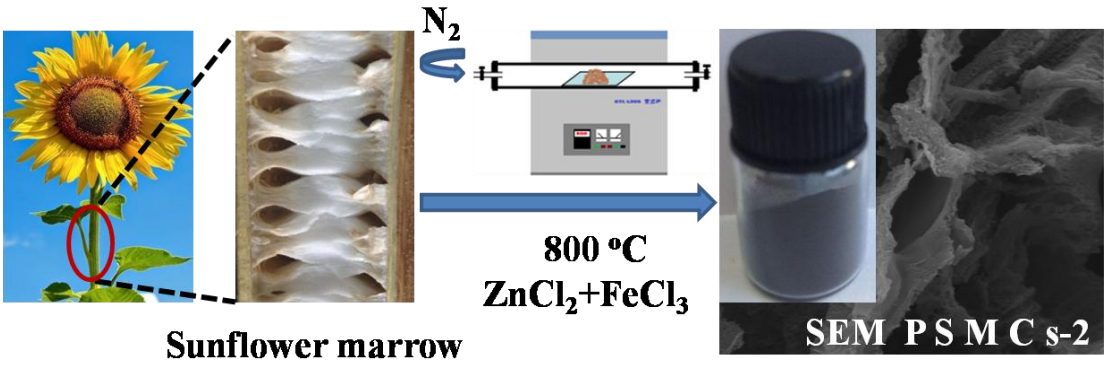

Scheme 1. Schematic of the preparation process of PSMCs-x materials.

2.3 Characterization

The surface morphology of the porous carbon materials were examined by field emission scanning electron microscopy (FE-SEM, Ultra Plus, Carl Zeiss). The specific surface areas were calculated by multiple points Brunauer-Emmett-Teller (BET) method, and the pore size distributions were estimated according to Barrett-Joyner-Halenda (BJH) theory. The Brunauer-Emmett-Teller surface area (S_{BET}) of the powders was analyzed by nitrogen adsorption in a Micromeritics ASAP 2020 nitrogen adsorption apparatus (U.S.A.). X-ray diffraction (XRD) was obtained from ground-up samples of the fibers using a Rigaku D-Max-2400 diffractometer and CuKa radiation (k =1.5418 Å) at 40 kV, 100 mA. The 2θ measure range was from 5 to 80°.The nitrogen adsorptiondesorption isotherms were measured on a Micromeritics Gemini 2380 surface area analyzer at 77 K. Raman spectra were recorded with an Invia Raman spectrometer (Renishaw) with an Argon ion laser (λ = 514 nm). The elemental microanalysis (C, H and N) was carried out using the Elemental Analyzer Vario EL.

2.4 Three-electrode system fabrication

Three-electrode configuration was adopted to evaluate the capacitive performance of the as-prepared activated materials on a CHI 660C electrochemical workstation (Shanghai ChenHua

Instruments Co., China). The test was performed in 2 M KOH aqueous electrolyte solution under ambient conditions. A high purity carbon rod serves and mercuric oxide electrode were used as the counter electrode and reference electrode, respectively. Typically, 4 mg of as-prepared products was ultrasonically dispersed in 0.4 mL of 0.25 wt% Nafion (DuPont, USA) ethanol solutions. The above suspension of 8 μL using a pipet gun was dropped onto the glassy carbon electrode and dried at room temperature. The active materials were weighted accurately for specific capacitances calculation.

2.5 Two-electrode cell fabrication

The capacitive performance of PSMCs was further investigated using a two-electrode testing cell. The working electrode was prepared by mixing 80 wt% PSMCs, 10 wt% acetylene black, and 10 wt% polyvinylidene fluoride (PVDF) binder in N-methyl-2-pyrrolidinone (NMP) solvent. The slurry was spread onto a diameter of 1.0 cm^{-2} nickel foam and dried at 60 ^{o}C overnight, then weighted and pressed into sheets under 10 MPa. The typical mass loading of active material was 0.3-0.5 mg cm^{-2}. Two as-prepared PSMCs electrodes fitted with the separator (thin polypropylene film) and electrolyte solution (0.5 mol L^{-1} Na_2SO_4 aqueous solutions) were symmetrically assembled into sandwich-type cells construction (electrode/separator/electrode). All the electrochemical tests were conducted at room temperature.

2.6 Electrochemical measurements

The electrochemical properties of the samples were investigated by cyclic voltammetry (CV), galvanostatic charge/discharge and electrochemical impedance spectroscopy (EIS) measurements in three-electrode system and two-electrode cell using a CHI 760E electrochemical workstation (Shanghai Chenghua instrument Co., Ltd, China). The cycle-life stability was performed using computer controlled cycling equipment (LAND CT2001A, Wuhan China). The EIS measurements frequency ranging from 10 mHz to 100 kHz and an impedance amplitude of ±5 mV at open circuit potential.

The gravimetric capacitance from galvanostatic charge/discharge was calculated by using the formula of $C_s=I\Delta t/(m\Delta V)$ for the three-electrode system, where I is the constant current (A) and m is the mass (g) of electrode material, Δt is the discharge time and ΔV is the voltage change during the discharge process.

3. RESULTS AND DISCUSSION

3.1. Microstructure characterizations

The morphological properties of PSMCs prepared in combination of $ZnCl_2$ and different concentration of $FeCl_3$ solution (0~3 M) are show in Figure1 (a-f). From the Figure1 (a-f), we can conclude, when carbonize sunflower marrow only using the activating agent $ZnCl_2$, the obtained PSMCs-0 is displayed irregular poor porosity holes shape with a rough surface (Figure 1a).

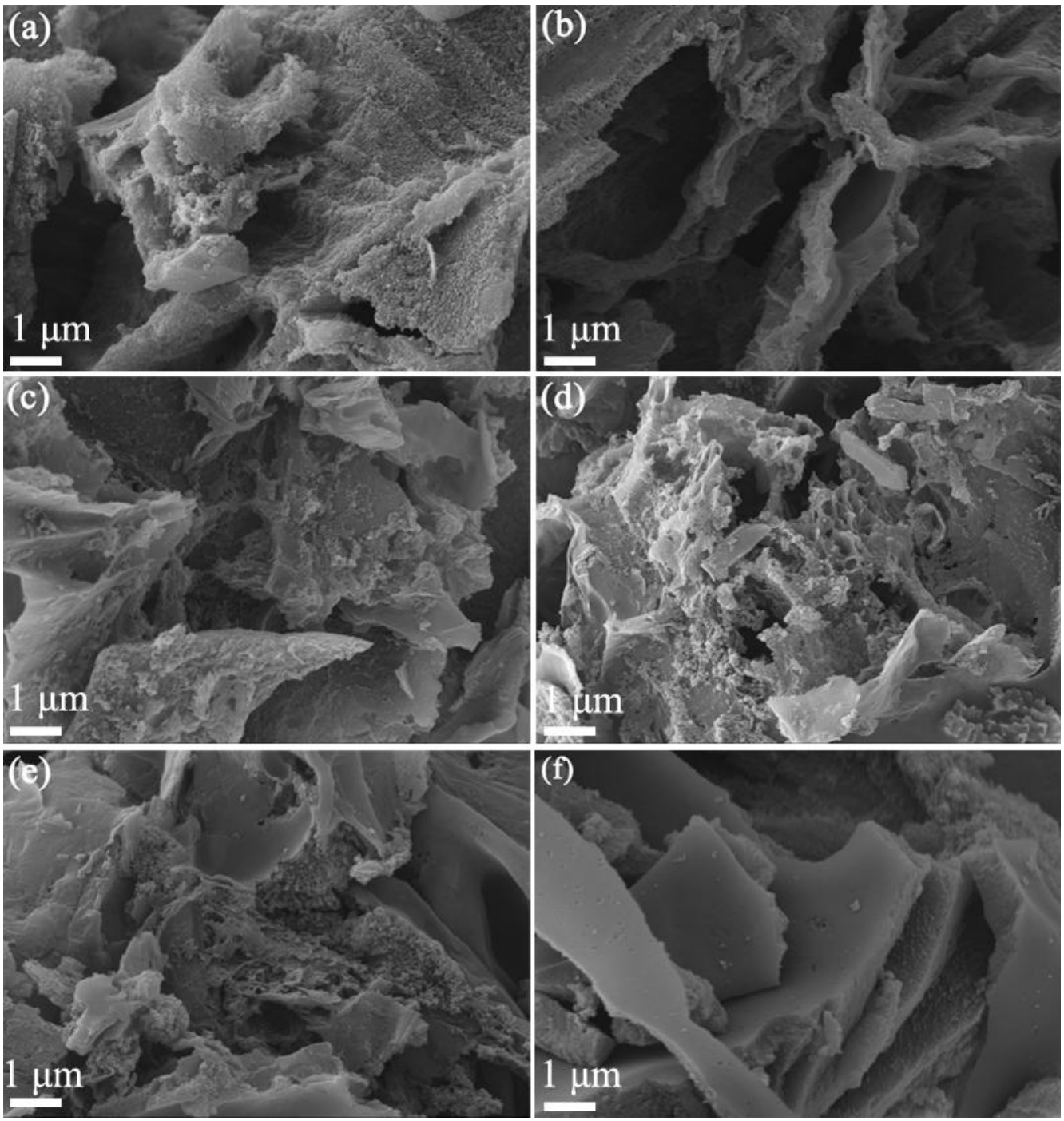

Figure 1. FE-SEM images of PSMCs-x prepared at different at different concentration of $FeCl_3$ solution: (a) PSMCs-0; (b) PSMCs-1; (c-d) PSMCs-2; (e) PSMCs-3; (f) PSMCs-c.

When the activating agent $ZnCl_2$ and low concentration of $FeCl_3$ solution (1 M) were incorporated simultaneously into the sunflower marrow, PSMCs-1 with abundant loose porous and three-dimensional network structure can be obtained (Figure 1b). More interestingly, when the activating agent $ZnCl_2$ and high concentration of $FeCl_3$ solution (2 M and 3M) were incorporated simultaneously into the sunflower marrow, the morphology of PSMCs-2 and PSMCs-3 is present more fluffy reticular and local areas sheet-like structure (Figure 1c-e). The PSMCs-c, sunflower marrow

with only $FeCl_3$ catalyst (3 M), is present a stacking sheet-like structure as shown in Figure 1f. Those experimental phenomena indicate that the $FeCl_3$ play an important role in the carbonation process, and the carbon pore structure could be controllable achieved by change the activating condition.

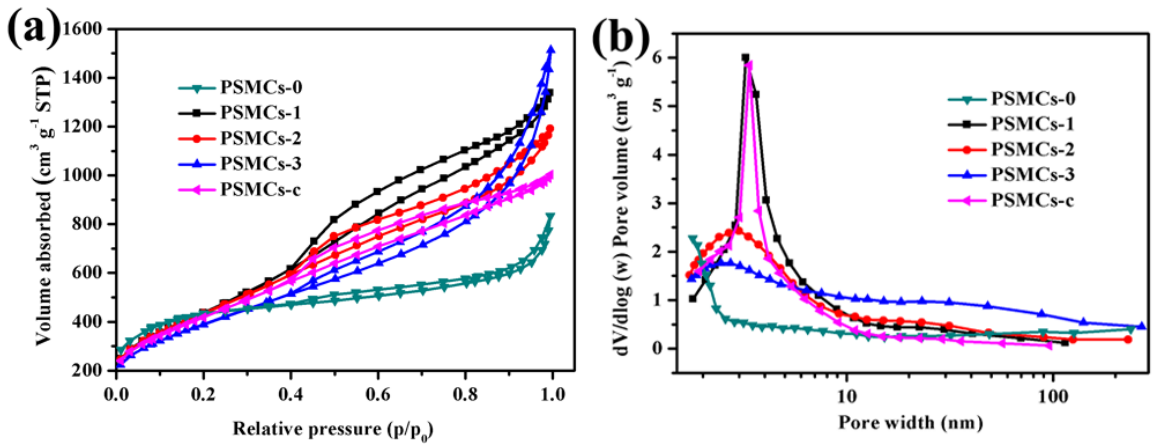

Figure 2. (a) Nitrogen adsorption-desorption isotherms and (b) pore size distribution curves of PSMCs-x prepared at different concentration of $FeCl_3$ solution.

Porosity of the PSMCs obtained under different process was analyzed by N_2 sorption technique. As shown in the Figure 2a, the N_2 adsorption-desorption isotherms of PSMCs are obtained by $ZnCl_2$ activation with various concentration $FeCl_3$ solutions ranging from 0 to 3 M. And the results indicate that $FeCl_3$ could greatly enhance the pore development of carbon samples during the chemistry activation.

Table 1. Elemental analysis, BET surface area and pore structure characterization parameters of 3D N-CNWs from different carbonization temperature.

Samples	Methods	S_{BET} [a)] ($m^2\ g^{-1}$)	Pore volume [b)] ($cm^3\ g^{-1}$)	Average pore [c)] size (nm)
PSMCs-0	$ZnCl_2$	1428.9	1.55	3.7
PSMCs-1	$ZnCl_2$ + 1 M $FeCl_3$	1554.0	1.84	5.0
PSMCs-2	$ZnCl_2$ + 2 M $FeCl_3$	1628.5	2.34	4.5
PSMCs-3	$ZnCl_2$ + 3 M $FeCl_3$	1562.5	2.06	6.5
PSMCs-c	3 M $FeCl_3$	1389.8	1.29	4.0

a) Specific surface area determined according to BET (Brunauer-Emmett-Teller) method.
b) Total pore volume at P/P0=0.99.
c) Average pore size.

The nitrogen adsorption isotherms of PSMCs-2 and PSMCs-3 have evident type IV with a H3 hysteresis loop, which can be observed in the adsorption/desorption isotherms, indicating the existence of mesopore size in modified activated carbons after $ZnCl_2$ and $FeCl_3$ activation [21,22]. Furthermore, sharp increases in volume at low relative pressure (P/P0< 0.4), especially the PSMCs-2 and PSMCs-3

prepared in higher concentration $FeCl_3$ solution (2 and 3 mol/L) indicate the presence of obvious mecropores. Therefore, it is reasonable to conclude that appropriate concentration of $FeCl_3$ solution can increase the BET specific surface area and pore volume increases of carbons. The pore size of PSMCs-2 calculated by the Barrett-Joyner-Halenda (BJH) model is shown in Figure 2b, indicated that the pore size of PSMCs-2 centered at 4.5 nm. Comparing with other samples, PSMCs-2 has a larger specific surface area and mecropore volume, which makes a significant contribution to high specific capacitance.

Table 1 summarizes the pore structural nature of PSMCs-x obtained by the nitrogen adsorption isotherms at 77 K. Only the activating agent ($ZnCl_2$) or combination with low concentration of $FeCl_3$ solution (1 M) used in the synthesis, both PSMCs-0 and PSMCs-1 exhibit a relatively low pore volumes. Under this prepared condition, their pore structure is mainly composed of the mecropores or small masopores. In particular, the BET surface area and total pore volume of PSMCs-2 are 1628 $m^2 g^{-1}$ and 2.34 $cm^3 g^{-1}$, respectively. However, when carbonize sunflower marrow with only $FeCl_3$ catalyst (3 M), the PSMCs-c displays a lower BET surface area (1389 $m^2 g^{-1}$) and pore volume (1.29 $cm^3 g^{-1}$). The large specific surface area and appropriate porous structure are in favor of quick mass charge transfer and ion diffusion, further leading to higher capacitance storage and rate capability.

The structure of the prepared PSMCs-2 was investigated by XRD and Raman spectroscopy, as shown in Figure 3. Figure 3a is the representative XRD pattern of the PSMCs-2. Obviously, two broad peaks at $2\theta = 22.6^o$ and 43.7^o are observed in the honeycomb networks structure carbon, ascribing to the (002) and (100) crystal planes of graphitic carbon, suggesting that PSMCs-2 is made of amorphous carbon and few graphitic carbon [23].

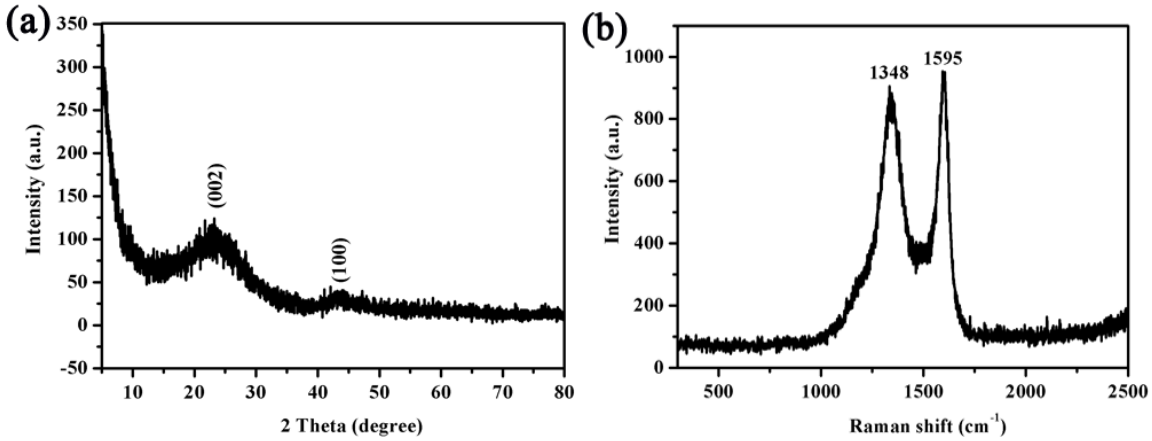

Figure 3. (a) XRD pattern and (b) Raman spectra of PSMCs-2.

The broad (002) diffraction peak centered at around 22.6^o of PSMCs-2 is in corresponding with interlayer spacing (0.392 nm), which is larger than natural graphite (0.335 nm). Figure 2b shows the Raman spectra of the PSMCs-2. These two prominent peaks at 1348 (D-band) and 1595 cm^{-1} (G-band) are to provide information about the crystallography and structure of the PSMCs-2. The D-band is associated with amorphous carbon structure, while the G-band is attributed to the vibration of all sp^2 hybridized carbon atoms in both rings and chains [24]. Moreover, because of the highly porous and

disordered structure caused by chemical activation, the I_G/I_D intensity ratio of PSMCs-2 is 0.85, indicating it is a long-range graphitized carbon with relatively little structural defects, which is in good agreement with results of XRD.

3.2. Electrochemical behavior and characterization

As presented in Figure 4, the electrochemical properties of the as-prepared PSMCs-x were evaluated in 2.0 M KOH aqueous solution by three-electrode system. The cyclic voltammograms (CV) curves of the PSMCs-x maintain quasi-rectangular shapes at a scan rate of 50 mV s^{-1} (Figure 4a), which indicated the PSMCs-x materials show the ideal capacitive behavior. Figure 4b shows the typical galvanostatic charge-discharge (CD) profiles of the as-prepared PSMCs-x at the current density of 1 A g^{-1}. Obviously, the PSMCs-2 possesses larger capacitive performance than other carbons, mainly owing to the larger charge-discharge time. Figure 4c shows the CVs of PSMCs-2 sample at scan rates of 10-100 mV s^{-1}, the plateau current increases accordingly with scan rate and the quasi-rectangular shape can be largely retained only with little distortion when the scan rate is up to 100 mV s^{-1}, indicating the good rate capability due to the low inner resistance. The specific capacitance of PSMCs-2 at various current densities can be estimated by galvanostatic charging-discharging times. As shown in Figure 4d, within current densities of 0.5-10 A g^{-1}, all the charging-discharging curves show symmetric triangular shape with linear voltage vs time profile, indicating little internal resistance and high rate capability of the PSMCs-x as supercapacitor electrode material. The specific capacitances of active electrode materials can be calculated according to the following equation: $C_m = It/(\Delta Vm)$. The specific capacitance value of the PSMCs-2 is as high as 232.5 F g^{-1} at a current density of 1 A g^{-1}, which indicates the fluffy reticular and porous structure can enhance the kinetics of ion and electron transportation in electrodes and at the electrode/electrolyte interface. The Nyquist plots for the PSMCs-2 shown in Figure 4e. It can been found, the impedance spectra of the PSMCs-2 contain a distorted semicircle in the high frequency region due to porosity of the sample and a linear part at the low frequency region due to diffusion-controlled doping and undoping of anions that result from Warburg behavior [25]. The high frequency intercept in the semicircle with the real axis gives the internal resistance value of these cell capacitors [26]. The low frequency, the imaginary part of the impedance is a nearly vertical line, which is a characteristic of capacitive behavior. All of the above results indicate the carbons have good electronic conductivity and electrochemical performances.

The discharge capacitances at various current densities of the PSMCs-2 are presentd in Figure 4f. It is evident that the capacitance slowly decreased with the increase of current densities. Its capacitance value is as high as 252.5 and 176.5 F g^{-1} at a current density of 0.5 and 20 A g^{-1}, about 70% capacitance retention.

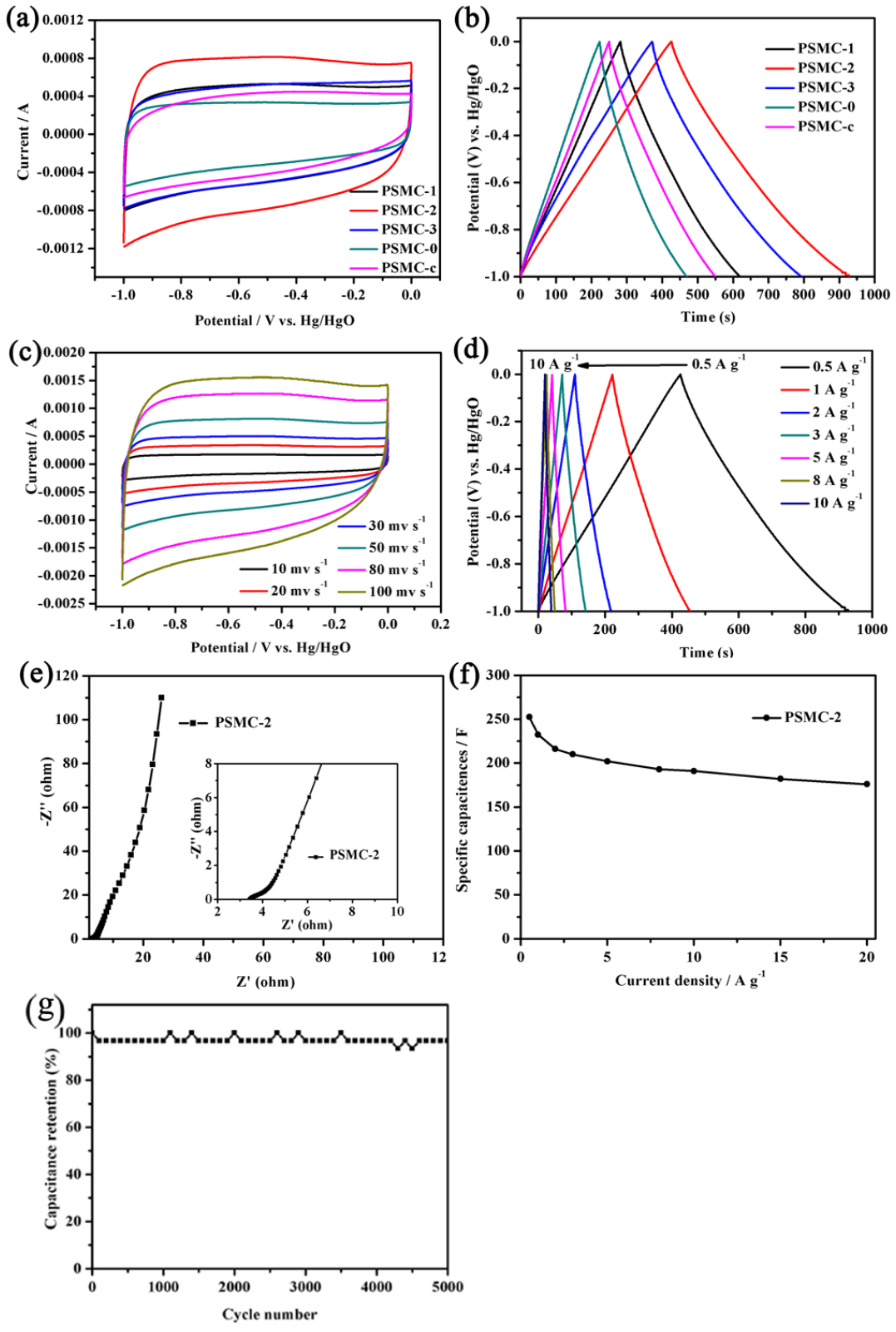

Figure 4. (a) Cyclic voltammograms (CVs) of different electrodes at a scan rate of 50 mV s^{-1} in 2 M KOH aqueous solution. (b) Charge-discharge curves of PSMCs at the current density of 0.5 A g^{-1}. (c) CV curves of PSMCs-2 electrode at different scan rates from 10 to 100 mV s^{-1} between -1 and 0 V (vs. Hg/HgO). (d) Discharge capacitances of PSMCs-2 at various current densities. (e) Nyquist plots base on PSMCs-2 electrodes. (f) Specific capacitances of PSMCs-2 at various current densities. (g) Cycling stability of the PSMCs-2.

The result indicates that the PSMCs-2 from sunflower marrow exhibits excellent electrochemical performance especially even at very high current density. Furthermore, the durability of the PSMCs-2 electrode has been characterized the long-term charge/discharge behavior by using galvanostatic charge/discharge measurement at a current density of 1.0 A g^{-1}. Figure 4g displays the capacitance retentions versus cycle number curves of PSMCs-2 at a current density of 5 A g^{-1} for 5000 cycles. As can be seen, the specific capacitance decreases slightly and remains about 97% of the initial capacitance after 5000 cycles. These results demonstrate that the activated carbons derived from sunflower marrow exhibit better cycle stability and a very high degree of reversibility during repetitive charge/discharge cycles in organic electrolytes.

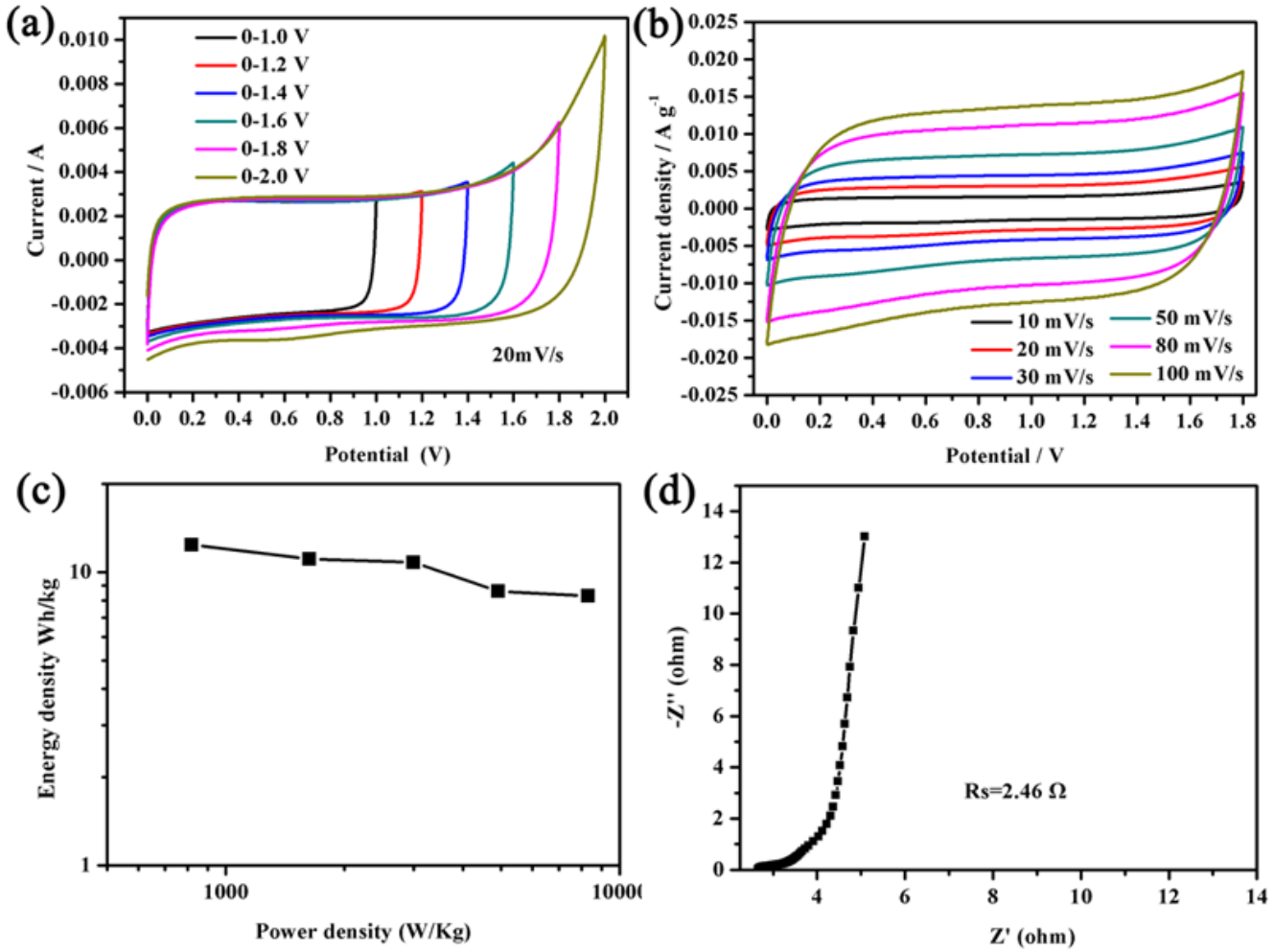

Figure 5. (a) CV curves of the PSMCs-2 symmetric two-electrode cell at different voltage windows in 0.5 M Na_2SO_4 aqueous electrolytes; (b) CV curves of the PSMCs-2 electrode at various scan rates;(c) Ragone plot of the PSMCs-2//PSMCs-2 symmetric cell in comparison to carbon based aqueous symmetric cells recently reported in the literature. (d) Nyquist plots of the PSMCs-2//PSMCs-2.

A two-electrode symmetric supercapacitor PSMCs-2//PSMCs-2 was fabricated to investigate the electrochemical performance of the PSMCs-2 electrode further. Figure 5a shows the CV curves at the scan rate of 20 mV s^{-1} in various voltage ranges of PSMCs-2 symmetric supercapacitor. Obviously,

the CV curves still maintain the rectangular-like shape and with no obvious distortion in the anodic current even the voltage up to 1.8 V, indicating ideal capacitive behavior and good reversibility. When the operating voltage increases to 2.0 V, however, the current is sharply increased since the electrolyte could be decomposed to hydrogen and/or oxygen. Therefore, the detailed investigation of PSMCs-2//PSMCs-2 symmetric supercapacitor is performed in the voltage range of 0-1.8 V.

The typical CV curves at different scan rates from 10 to 200 mV s^{-1} are displayed in Figure 5b. It can be observed that the CV curves still exhibit rectangular shape even at a scan rate of 100 mV s^{-1}. Figure 5c shows the Ragone plot of the PSMCs-2//PSMCs-2 and symmetric supercapacitors in the potential range of 0-1.8 V. The PSMCs-2//PSMCs-2 symmetric cell exhibits the highest energy density is 12.4 Wh Kg^{-1} at a power density of 817 W Kg-1 and even remained 8.3 Wh Kg^{-1} at a power density of 8300 W Kg^{-1}. These results demonstrate that the PSMCs-2 material could be a promising electrode material in supercapacitors. The Nyquist plot of the PSMCs-2//PSMCs-2 symmetric supercapacitor is shown in Figure 5d. In the high-frequency region, the imaginary part (Z′) of the impedance is very small and the real part of resistance (Z″) is in corresponding with the ohmic resistance from the electrolyte and the interface between the current collector and the active material (Rs). And the nearly vertical line curve represents the ideal capacitive behavior of the carbon material in the low-frequency region [27]. As shown in Figure 5d, the internal resistance of PSMCs-2 is 2.46 Ω, indicating high electrical conductivity of the test symmetric cell.

Finally, to demonstrate the practical application of PSMCs-2, PSMCs-2//PSMCs-2 supercapacitors has been assembled. After being charged to 3 V for about 30 s, two devices were connected in series to light red emitting diodes (LED, working voltage: 1.5 V) as shown in inset of Figure 5c. Here we found that two devices could light a red light-emitting diode for ≈ 4 min after charging at 5 A g^{-1} for 30 s, exhibiting high energy density and fast charge ability.

4. CONCLUSION

In this paper, we have prepared a fluffy reticular porous carbon materials using biomass by $ZnCl_2$ and $FeCl_3$ as activation agent. The high specific surface area and controllable pore size are beneficial for the high capacitive performance of the as-prepared PSMCs-2. As an electrode material for supercapacitors, the PSMCs-2 electrode possesses a large specific capacitance of 252.5 F g^{-1} at 0.5 A g^{-1}. Furthermore, PSMCs symmetric supercapacitor exhibits specific energies of 12.4 Wh kg^{-1} at a power density of 817 W kg^{-1} in 0.5 M Na_2SO_4 aqueous electrolyte and in the voltage range of 0-1.8 V. Furthermore, it retains about 97% initial capacitance after 5000 cycles, indicating excellent cycle ability. Due to the good cycling stability, excellent long term reliability, high specific capacitance and superior capacitance maintaining ability, PSMCs supercapacitor displays huge potential in cost-effective and high-performance energy storage devices.

ACKNOWLEDGEMENT
This research was financially supported by the National Science Foundation of China (21664012, 51462032), the program for Changjiang Scholars and Innovative Research Team in University

(IRT15R56), Innovation Team Basic Scientific Research Project of Gansu Province (1606RJIA324), Key Laboratory of Eco-Environment-Related Polymer Materials of Ministry of Education, and Key Laboratory of Polymer Materials of Gansu Province. H. Peng thanks the financial support provided by the Outstanding Doctoral Dissertation Cultivation Program of Northwest Normal University.

References

1. J. Chang, Z. Gao, X. Wang, D. Wu, F. Xu, X. Wang, K. Jiang, *Electrochim. Acta*, 1 (2015) 290-298.
2. Y. Qiu, G. Li, Y. Hou, Z. Pan, H. Li, W. Li, Y. Zhang, *Chem. Mater.*, 27 (2015) 1194-1200.
3. K. Srirangan, L. Akawi, M. Moo-Young, C. P. Chou, *Appl. Energ.*, 100 (2012) 172-186.
4. K. Wang, N. Zhao, S. Lei, R. Yan, X. Tian, J. Wang, L. Liu, *Electrochim. Acta*, 166 (2015) 1-11.
5. J. Yan, Q. Wang, T. Wei, Z. Fan, *Adv. Energy Mater.*, 4 (2014) DOI: 10.1002/aenm.201300816.
6. J. Zhi, W. Zhao, X. Liu, A. Chen, Z. Liu, F. Huang, *Adv. Funct. Mater.*, 24 (2014) 2013-2019.
7. S. Faraji, F. N. Ani, *Renew. Sust. Energ. Rev.*, 42 (2015) 823-834.
8. G. Ren, G. Ma, N. Cong, *Renew. Sus. Energ. Rev.*, 41 (2015) 225-236.
9. G. Wang, J. Zhang, S. Kuang, J. Zhou, W. Xing, S. Zhuo, *Electrochim. Acta*, 153 (2015) 273-279.
10. X. Yang, J. Zhu, L. Qiu, D. Li, *Adv. mater.*, 23 (2011) 2833-2838.
11. M. Kodama, J. Yamashita, Y. Soneda, H. Hatori, S. Nishimura, K. Kamegawa, *Mater. Sci. Eng. B*, 108 (2004) 156-161.
12. H. M. Luo, Y. F. Yang, Y. X. Sun, X. Zhao, J. Q. Zhang, *J. Solid State Electr.*, 19 (2015) 1491-1500.
13. R. K. Emmett, M. Karakaya, R. Podila, M. R. Arcila-Velez, J. Zhu, A. M. Rao, M. E. Roberts, *J. Phys. Chem. C*, 118 (2014) 26498-26503.
14. F. Markoulidis, C. Lei, C. Lekakou, D. Duff, S. Khalil, B. Martorana, I. Cannavaro, *Carbon*, 68 (2014) 58-66.
15. M. K. Singh, M. Suleman, Y. Kumar, S. A. Hashmi, *Energy*, 80 (2015) 465-473.
16. T. Zhang, F. Zhang, L. Zhang, Y. Lu, Y. Zhang, X. Yang, Y. Huang, *Carbon*, 92 (2015) 106-118.
17. G. G. Choi, S. J. Oh, S. J. Lee, J. S. Kim, *Bioresource Technol.*, 178 (2015) 99-107.
18. E. Redondo, J. Carretero-González, E. Goikolea, J. Ségalini, R. Mysyk, *Electrochim. Acta*, 160 (2015) 178-184.
19. M. Chen, X. Kang, T. Wumaier, J. Dou, B. Gao, Y. Han, L. Zhang, *J. Solid State Electr.*, 17 (2013) 1005-1012.
20. K. Wang, N. Zhao, S. Lei, R. Yan, X. Tian, J. Wang, L. Liu, *Electrochim. Acta*, 166 (2015) 1-11.
21. H. Binici, M. Eken, M. Dolaz, O. Aksogan, M. Kara, *Constr. Build. Mater.*, 51 (2014) 24-33.
22. Y. Yang, B. Zhao, P. Tang, Z. Cao, M. Huang, S. Tan, *Carbon*, 77 (2014) 113-121.
23. H. Peng, G. Ma, K. Sun, J. Mu, Z. Zhang, Z. Lei, *ACS Appl. Mater. inter.*, 6 (2014) 20795-20803.
24. X. Huang, S. Kim, M. S. Heo, J. E. Kim, H. Suh, I. Kim, *Langmuir*, 29 (2013) 12266-12274.
25. M. Chen, X. Kang, T. Wumaier, J. Dou, B. Gao, Y. Han, L. Zhang, *J Solid State Electr.*, 17 (2013) 1005-1012.
26. Z. Fan, J. Yan, T. Wei, L. Zhi, G. Ning, T. Li, F. Wei, *Adv. Funct. Mater.*, 21 (2011) 2366-2375.
27. J. Yan,T. Wei, B. Shao, F. Ma, Z. Fan, M. Zhang, C. Zheng, Y. Shang, W. Qian, F. Wei, *Carbon*, 48 (2010) 1731-1737.